

Nonlinear Dual-Mode Control of Variable-Speed Wind Turbines with Doubly Fed Induction Generators

Choon Yik Tang, *Member, IEEE*, Yi Guo, *Student Member, IEEE*, and John N. Jiang, *Senior Member, IEEE*

Abstract—This paper presents a feedback/feedforward nonlinear controller for variable-speed wind turbines with doubly fed induction generators. By appropriately adjusting the rotor voltages and the blade pitch angle, the controller simultaneously enables: (a) control of the active power in both the *maximum power tracking* and *power regulation* modes, (b) seamless switching between the two modes, and (c) control of the reactive power so that a desirable power factor is maintained. Unlike many existing designs, the controller is developed based on original, nonlinear, electromechanically-coupled models of wind turbines, without attempting approximate linearization. Its development consists of three steps: (i) employ feedback linearization to exactly cancel some of the nonlinearities and perform arbitrary pole placement, (ii) design a speed controller that makes the rotor angular velocity track a desired reference whenever possible, and (iii) introduce a Lyapunov-like function and present a gradient-based approach for minimizing this function. The effectiveness of the controller is demonstrated through simulation of a wind turbine operating under several scenarios.

Index Terms—Wind energy, wind turbine, active power, reactive power, maximum power tracking, power regulation, nonlinear control.

I. INTRODUCTION

WIND power is gaining ever-increasing attention in recent years as a clean, safe, and renewable energy source. With the fast growth of wind generation in power systems, wind power is becoming a significant portion of the generation portfolio in the United States as well as many countries in Europe and Asia [1]. Indeed, wind power penetration is planned to surpass 20% of the United States' total energy production by 2030—a figure that is way beyond the current level of less than 5% [2]. Hence, to realize this vision, it is necessary to develop large-scale wind farms that effectively produce electric power from wind, and integrate them with the power systems.

The integration of large-scale wind farms into a power system, however, changes the fundamental principle of its operation, which is to maintain reliability by balancing load variation with “controllable” generation resources. When a portion of these resources comes from “uncontrollable” wind generation, that portion of the resources can hardly be guaranteed due to the intermittency of wind. As a result, the power system may fail to achieve the required balance. When

the level of wind power penetration is small, this issue may be safely neglected. However, with the anticipated increase in penetration, the issue becomes critical for power system reliability. As a case in point, half of the European grids experienced a severe difficulty in 2006 because several large wind farms, operating in the *maximum power tracking* (MPT) mode, produced excessive power that destabilized the grids. This event took place even though the wind penetration level, at that time, was low at only 7% [3].

Such an experience suggests that it is not advisable—and may be even disastrous—for a large-scale wind farm connected to a grid to always operate in the MPT mode, making wind turbines in the farm harvest as much wind energy as they possibly could, following the “let it be when the wind blows” philosophy of operation. Instead, it is highly desirable that the wind farm can also operate in the *power regulation* (PR) mode, whereby its total power output from the wind turbines is closely regulated at some desired setpoint, despite the fluctuating wind conditions.

The ability to operate in the PR mode in addition to the MPT mode, as well as the ability to *seamlessly* switch between the two, offers many important advantages: not only does the PR mode provide a cushion to absorb the impact of wind fluctuations on total power output through power regulation, it also enables a power system to effectively respond to changes in reliability conditions and economic signals. For instance, when a sudden drop in load occurs, the power system may ask the wind farm to switch from the MPT to the PR mode and generate less power, rather than rely on expensive down-regulation generation. As another example, the PR mode, when properly designed, allows the power output of a wind farm to smoothly and accurately follow system dispatch requests, thus reducing its reliance on ancillary services such as reliability reserves.

To enable large-scale wind farms to operate well in these two modes and switch seamlessly between them, numerous challenges must be overcome. This paper is devoted to addressing a subset of these challenges, by presenting an integrated framework for controlling the rotor voltages and the blade pitch angle of variable-speed wind turbines with doubly fed induction generators (DFIGs). The paper presents a feedback/feedforward nonlinear controller developed based on original, nonlinear, and electromechanically-coupled models of wind turbines, without attempting approximate linearization. The controller simultaneously enables: (a) control of the active power in both the MPT and PR modes, (b) seamless

The authors are with the School of Electrical and Computer Engineering, University of Oklahoma, Norman, OK 73019 USA (e-mail: {cvtang,yi.guo,jnjiang}@ou.edu).

This work was supported by the National Science Foundation under grants ECCS-0926038 and ECCS-0955265.

switching between the two modes, and (c) control of the reactive power so that a desirable power factor is ensured. Its development consists of three steps. First, we show that, although dynamics of a wind turbine are highly nonlinear and electromechanically coupled, they offer a structure, which makes the electrical part feedback linearizable, so that arbitrary pole placement can be carried out. Second, we show that because the electrical dynamics can be made very fast, it is possible to perform model order reduction, so that only the first-order mechanical dynamics remain to be considered. For this reduced first-order model, a speed controller is designed, which enables the rotor angular velocity to track a desired reference whenever possible. Finally, we introduce a Lyapunov-like function that measures the difference between the actual and desired powers and present a gradient-based approach for minimizing this function. The effectiveness of the controller is demonstrated through simulation of a wind turbine operating under a changing wind speed, changing desired power outputs, modeling errors, and noisy measurements.

To date, a significant amount of research has been performed on the control of variable-speed wind turbines [4]–[37]. The existing publications, however, are substantially different from our work in the following aspects:

- (i) The mechanical and electrical parts of the wind turbines are considered separately in most of the current literature: [4]–[21] considered only the mechanical part, while [22]–[36] considered only the electrical part, focusing mostly on the DFIGs. In contrast, in this paper we consider *both* the mechanical and electrical parts. Although [37] also considered both these parts, its controller was designed to maximize wind energy conversion, as opposed to achieving power regulation (i.e., only operate in the MPT mode). In comparison, our controller can operate in *both* the MPT and PR modes as well as seamlessly switch between the two.
- (ii) For those references [4]–[21] considering only the mechanical part, control of the active power has been the main focus: [4], [5] maximized the wind power capture at low to medium wind speeds by adjusting both the generator torque and the blade pitch angle, [6]–[9] did the same by adjusting only the generator torque, and [13]–[21] aimed to maintain the rated rotor speed and limit the power production at high wind speeds by controlling the blade pitch angle. Although the results are interesting, there is a lack of discussion on reactive power control, which is sometimes crucial to power system reliability. On the other hand, for those references [22]–[36] considering only the electrical part, [22], [23] considered only the active power control, while [24]–[27] dealt with the reactive power. In contrast, we provide an integrated solution to the more difficult problem of simultaneously controlling *both* the active and reactive powers by appropriately adjusting *both* the rotor voltages and the blade pitch angle.
- (iii) From a modeling point of view, the wind turbine model we consider is one of the most comprehensive. Specifically, [12]–[14] assumed a linearized model of the me-

chanical torque from wind turbines, while [4]–[11], [15] considered a nonlinear one. In addition, [23]–[32], [35]–[37] considered a reduced-order DFIG model, while [33], [34] considered a full-order one. In contrast, we consider a fifth-order, nonlinear, electromechanically-coupled model and attempt no linearization around some operating points.

- (iv) Finally, from a controls point of view, the control techniques we use are different from those adopted in [4]–[37]. For control of the mechanical part of the wind turbines, several techniques have been considered, including proportional-integral-derivative (PID) [12]–[14], fuzzy control [4], [8]–[10], [21], adaptive control [6], [7], robust nonlinear control [5], [15], sliding mode control [11], and wind-model-based predictive control [17]. Similarly, for control of the electrical part, various ways of controlling the DFIGs have been proposed, including vector/decoupling control with or without a position encoder [23]–[25], [31], [32], [34]–[37], direct power control [28], power error vector control [30], robust coordinated control [26], linear quadratic regulator [29], nonlinear inverse system method [27], and passivity-based control [33]. In comparison, the controller we propose here consists of a mixture of several linear/nonlinear control techniques, including feedback linearization, pole placement, and gradient-based optimization and involving three time scales. The reason our controller is more complex is that the problem we address is inherently more challenging (see (i) and (ii)) and the model is more comprehensive (see (i) and (iii)).

As it follows from the above brief review of the current literature, this paper contributes significantly to the state of the art on the control of wind turbines.

The remainder of the paper is organized as follows: Section II describes a model of variable-speed wind turbines with DFIGs. Section III introduces the proposed feedback/feedforward nonlinear controller. Simulation results are shown in Section IV. Finally, Section V concludes the paper.

II. MODELING

Consider a variable-speed wind turbine consisting of a doubly fed induction generator (DFIG) and a power electronics converter, as shown in Figure 1. The DFIG may be regarded as a slip-ring induction machine, whose stator winding is directly connected to the grid, and whose rotor winding is connected to the grid through a bidirectional frequency converter using back-to-back PWM voltage-source converters.

The dynamics of the electrical part of the wind turbine are represented by a fourth-order state space model, constructed using the synchronously rotating reference frame (dq -frame), where the relation between the three phase quantities and the dq components is defined by Park's transformation [38]. The voltage equations are [39]

$$v_{ds} = R_s i_{ds} - \omega_s \varphi_{qs} + \frac{d}{dt} \varphi_{ds}, \quad (1)$$

$$v_{qs} = R_s i_{qs} + \omega_s \varphi_{ds} + \frac{d}{dt} \varphi_{qs}, \quad (2)$$

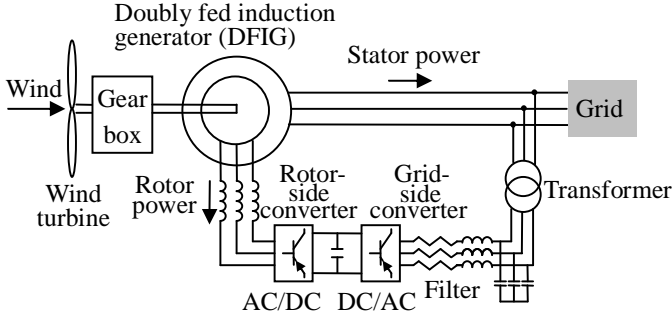


Fig. 1. Schematic of a typical variable-speed wind turbine with a DFIG.

$$v_{dr} = R_r i_{dr} - (\omega_s - \omega_r) \varphi_{qr} + \frac{d}{dt} \varphi_{dr}, \quad (3)$$

$$v_{qr} = R_r i_{qr} + (\omega_s - \omega_r) \varphi_{dr} + \frac{d}{dt} \varphi_{qr}, \quad (4)$$

where v_{ds} , v_{qs} , v_{dr} , v_{qr} are the d - and q -axis of the stator and rotor voltages; i_{ds} , i_{qs} , i_{dr} , i_{qr} are the d - and q -axis of the stator and rotor currents; φ_{ds} , φ_{qs} , φ_{dr} , φ_{qr} are the d - and q -axis of the stator and rotor fluxes; ω_s is the constant angular velocity of the synchronously rotating reference frame; ω_r is the rotor angular velocity; and R_s , R_r are the stator and rotor resistances. The flux equations are [39]

$$\varphi_{ds} = L_s i_{ds} + L_m i_{dr}, \quad (5)$$

$$\varphi_{qs} = L_s i_{qs} + L_m i_{qr}, \quad (6)$$

$$\varphi_{dr} = L_m i_{ds} + L_r i_{dr}, \quad (7)$$

$$\varphi_{qr} = L_m i_{qs} + L_r i_{qr}, \quad (8)$$

where L_s , L_r , and L_m are the stator, rotor, and mutual inductances, respectively, satisfying $L_s > L_m$ and $L_r > L_m$. From (5)–(8), the current equations can be written as

$$i_{ds} = \frac{1}{\sigma L_s} \varphi_{ds} - \frac{L_m}{\sigma L_s L_r} \varphi_{dr}, \quad (9)$$

$$i_{qs} = \frac{1}{\sigma L_s} \varphi_{qs} - \frac{L_m}{\sigma L_s L_r} \varphi_{qr}, \quad (10)$$

$$i_{dr} = -\frac{L_m}{\sigma L_s L_r} \varphi_{ds} + \frac{1}{\sigma L_r} \varphi_{dr}, \quad (11)$$

$$i_{qr} = -\frac{L_m}{\sigma L_s L_r} \varphi_{qs} + \frac{1}{\sigma L_r} \varphi_{qr}, \quad (12)$$

where $\sigma = (1 - \frac{L_m^2}{L_s L_r})$ is the leak coefficient. Selecting the fluxes as state variables and substituting (9)–(12) into (1)–(4), the electrical dynamics in state space form can be written as

$$\frac{d}{dt} \varphi_{ds} = -\frac{R_s}{\sigma L_s} \varphi_{ds} + \omega_s \varphi_{qs} + \frac{R_s L_m}{\sigma L_s L_r} \varphi_{dr} + v_{ds}, \quad (13)$$

$$\frac{d}{dt} \varphi_{qs} = -\omega_s \varphi_{ds} - \frac{R_s}{\sigma L_s} \varphi_{qs} + \frac{R_s L_m}{\sigma L_s L_r} \varphi_{qr} + v_{qs}, \quad (14)$$

$$\frac{d}{dt} \varphi_{dr} = \frac{R_r L_m}{\sigma L_s L_r} \varphi_{ds} - \frac{R_r}{\sigma L_r} \varphi_{dr} + (\omega_s - \omega_r) \varphi_{qr} + v_{dr}, \quad (15)$$

$$\frac{d}{dt} \varphi_{qr} = \frac{R_r L_m}{\sigma L_s L_r} \varphi_{qs} - (\omega_s - \omega_r) \varphi_{dr} - \frac{R_r}{\sigma L_r} \varphi_{qr} + v_{qr}. \quad (16)$$

Neglecting power losses associated with the stator and rotor resistances, the active and reactive stator and rotor powers are

given by [40]

$$P_s = -v_{ds} i_{ds} - v_{qs} i_{qs}, \quad (17)$$

$$Q_s = -v_{qs} i_{ds} + v_{ds} i_{qs}, \quad (18)$$

$$P_r = -v_{dr} i_{dr} - v_{qr} i_{qr}, \quad (19)$$

$$Q_r = -v_{qr} i_{dr} + v_{dr} i_{qr}, \quad (20)$$

and the total active and reactive powers of the turbine are

$$P = P_s + P_r, \quad (21)$$

$$Q = Q_s + Q_r, \quad (22)$$

where positive (negative) values of P and Q mean that the turbine injects power into (draws power from) the grid.

The dynamics of the mechanical part of the wind turbine are represented by a first-order model

$$J \frac{d}{dt} \omega_r = T_m - T_e - C_f \omega_r, \quad (23)$$

where C_f is the friction coefficient, T_m is the mechanical torque generated, and T_e is the electromagnetic torque given by [40]

$$T_e = \varphi_{qs} i_{ds} - \varphi_{ds} i_{qs}, \quad (24)$$

where positive (negative) values mean the turbine acts as a generator (motor). The mechanical power captured by the wind turbine is given by [41]

$$P_m = T_m \omega_r = \frac{1}{2} \rho A C_p(\lambda, \beta) V_w^3, \quad (25)$$

where ρ is the air density; $A = \pi R^2$ is the area swept by the rotor blades of radius R ; V_w is the wind speed; and $C_p(\lambda, \beta)$ is the performance coefficient of the wind turbine, whose value is a function [41] of the tip speed ratio λ , defined as

$$\lambda = \frac{\omega_r R}{V_w}, \quad (26)$$

as well as the blade pitch angle β , assumed to lie within some mechanical limits β_{\min} and β_{\max} . This function is typically provided by turbine manufacturers and may vary greatly from one turbine to another [41]. Therefore, to make the results of this paper broadly applicable to a wide variety of turbines, no specific expression of $C_p(\lambda, \beta)$ will be assumed, until it is absolutely necessary in Section IV, to carry out simulations. Instead, $C_p(\lambda, \beta)$ will only be assumed to satisfy the following mild conditions:

(A1) Function $C_p(\lambda, \beta)$ is continuously differentiable in both λ and β over $\lambda \in (0, \infty)$ and $\beta \in [\beta_{\min}, \beta_{\max}]$.

(A2) There exists $c \in (0, \infty)$ such that for all $\lambda \in (0, \infty)$ and $\beta \in [\beta_{\min}, \beta_{\max}]$, we have $C_p(\lambda, \beta) \leq c\lambda$. This condition is mild because it is equivalent to saying that the mechanical torque T_m is bounded from above, since $T_m \propto \frac{C_p(\lambda, \beta)}{\lambda}$ according to (25) and (26).

(A3) For each fixed $\beta \in [\beta_{\min}, \beta_{\max}]$, there exists $\lambda_1 \in (0, \infty)$ such that for all $\lambda \in (0, \lambda_1)$, we have $C_p(\lambda, \beta) > 0$. This condition is also mild because turbines are designed to capture wind power over a wide range of λ , including times when λ is small.

For the purpose of simulation in Section IV, the following model of $C_p(\lambda, \beta)$ will be assumed, which is presented in [42] and also adopted in MATLAB/Simulink R2007a:

$$C_p(\lambda, \beta) = c_1 \left(\frac{c_2}{\lambda_i} - c_3\beta - c_4 \right) e^{-\frac{c_5}{\lambda_i}} + c_6\lambda, \quad (27)$$

where

$$\frac{1}{\lambda_i} = \frac{1}{\lambda + 0.08\beta} - \frac{0.035}{\beta^3 + 1}, \quad (28)$$

and the coefficients are $c_1 = 0.5176$, $c_2 = 116$, $c_3 = 0.4$, $c_4 = 5$, $c_5 = 21$, and $c_6 = 0.0068$.

As it follows from the above, the wind turbine studied in this paper is described by a fifth-order nonlinear dynamical system with states $[\varphi_{ds} \varphi_{qs} \varphi_{dr} \varphi_{qr} \omega_r]^T$, controls $[v_{dr} v_{qr} \beta]^T$, outputs $[P Q]^T$, “disturbance” V_w , nonlinear state equations (13)–(16) and (23), and nonlinear output equations (17)–(22). Notice that the system dynamics are strongly coupled: the “mechanical” state variable ω_r affects the electrical dynamics bilinearly via (15) and (16), while the “electrical” state variables $[\varphi_{ds} \varphi_{qs} \varphi_{dr} \varphi_{qr}]^T$ affect the mechanical dynamics quadratically via (9)–(12), (24) and (23). Since the stator winding of the DFIG is directly connected to the grid, for reliability reasons $[v_{ds} v_{qs}]^T$ are assumed to be fixed, i.e., not to be controlled, in the rest of this paper. Moreover, since (9)–(12) represent a bijective mapping between $[\varphi_{ds} \varphi_{qs} \varphi_{dr} \varphi_{qr}]^T$ and $[i_{ds} i_{qs} i_{dr} i_{qr}]^T$ and since the currents $[i_{ds} i_{qs} i_{dr} i_{qr}]^T$, the rotor angular velocity ω_r , and the wind speed V_w can all be measured, a controller for this system has access to its entire states (i.e., full state feedback is available) and its disturbance (i.e., the wind speed V_w). A block diagram of this system is shown on the right-hand side of Figure 2.

III. CONTROLLER DESIGN

In this section, a feedback/feedforward nonlinear controller of the form depicted on the left-hand side of Figure 2 is presented. By adjusting the rotor voltages v_{dr} and v_{qr} and the blade pitch angle β , the controller attempts to make the active and reactive powers P and Q track, as closely as possible—limited only by wind strength—some desired, time-varying references P_d and Q_d , presumably provided by a wind farm operator. When P_d is set to sufficiently large, i.e., larger than what the turbine can possibly convert from wind, it means the operator wants the turbine to operate in the MPT mode; otherwise, the PR mode is sought. The value of Q_d , along with that of P_d , reflects a desired power factor $\text{PF}_d = \frac{P_d}{\sqrt{P_d^2 + Q_d^2}}$ the operator wants the turbine to also maintain.

The controller development consists of three steps, which are described in Sections III-A–III-C, respectively.

A. Feedback Linearization and Pole Placement

For convenience, let us introduce the variable $x = [x_1 \ x_2 \ x_3 \ x_4]^T = [\varphi_{ds} \ \varphi_{qs} \ \varphi_{dr} \ \varphi_{qr}]^T$ and rewrite (9)–(12)

and (13)–(16) in matrix forms as follows:

$$\dot{x} = \underbrace{\begin{bmatrix} -\frac{R_s}{\sigma L_s} & \omega_s & \frac{R_s L_m}{\sigma L_s L_r} & 0 \\ -\omega_s & -\frac{R_s}{\sigma L_s} & 0 & \frac{R_s L_m}{\sigma L_s L_r} \\ \frac{R_r L_m}{\sigma L_s L_r} & 0 & -\frac{R_r}{\sigma L_r} & \omega_s \\ 0 & \frac{R_r L_m}{\sigma L_s L_r} & -\omega_s & -\frac{R_r}{\sigma L_r} \end{bmatrix}}_A x + \begin{bmatrix} v_{ds} \\ v_{qs} \\ v_{dr} - \omega_r x_4 \\ v_{qr} + \omega_r x_3 \end{bmatrix}, \quad (29)$$

$$\begin{bmatrix} i_{ds} \\ i_{qs} \\ i_{dr} \\ i_{qr} \end{bmatrix} = \begin{bmatrix} \frac{1}{\sigma L_s} & 0 & -\frac{L_m}{\sigma L_s L_r} & 0 \\ 0 & \frac{1}{\sigma L_s} & 0 & -\frac{L_m}{\sigma L_s L_r} \\ -\frac{L_m}{\sigma L_s L_r} & 0 & \frac{1}{\sigma L_r} & 0 \\ 0 & -\frac{L_m}{\sigma L_s L_r} & 0 & \frac{1}{\sigma L_r} \end{bmatrix} x, \quad (30)$$

where A is a constant matrix and, as was pointed out at the end of Section II, both v_{ds} and v_{qs} are constants not to be controlled. Note that the only nonlinearities in (29) are the two products of the state variables, i.e., $-\omega_r x_4$ and $\omega_r x_3$. Also note that these nonlinearities appear on the same rows as the control variables v_{dr} and v_{qr} . Thus, *feedback linearization* [43] may be used to cancel them and subsequently perform arbitrary *pole placement* [44], i.e., let

$$v_{dr} = \omega_r x_4 - K_1^T x + u_1, \quad (31)$$

$$v_{qr} = -\omega_r x_3 - K_2^T x + u_2, \quad (32)$$

where $K_1, K_2 \in \mathbb{R}^4$, the first terms on the right-hand side of (31) and (32) are intended to cancel the nonlinearities, the second terms are for pole placement, and the third are new control variables u_1 and u_2 , to be designed later.

To implement (31) and (32), full state feedback on the fluxes x and the rotor angular velocity ω_r are needed. While the latter is relatively easy to measure, the former is not. Fortunately, this difficulty can be circumvented by first measuring the currents—which is feasible—and then calculating the fluxes from (5)–(8). This explains the fourth input of the *nonlinear controller* block in Figure 2.

Substituting (31) and (32) into (29) yields

$$\dot{x} = (A - BK)x + [v_{ds} \ v_{qs} \ u_1 \ u_2]^T, \quad (33)$$

where $B = [0_{2 \times 2} \ I_{2 \times 2}]^T$ and $K = [K_1 \ K_2]^T$ is the state feedback gain matrix. Since the electrical elements in the DFIG are physically allowed to have much faster responses than their mechanical counterparts, K in (33) may be chosen so that $A - BK$ is asymptotically stable with very fast eigenvalues. With this choice of K and with relatively slow-varying u_1 and u_2 (recall that v_{ds} and v_{qs} are constants), the fourth-order linear differential equation (33) may be approximated by the following static, linear equation:

$$x = -(A - BK)^{-1} [v_{ds} \ v_{qs} \ u_1 \ u_2]^T. \quad (34)$$

As a result, the fifth-order model described in (13)–(16) and (23) may be approximated by the first-order model described in (23) along with (34). As will be shown next, this approximation greatly simplifies the design of u_1 and u_2 . Therefore,

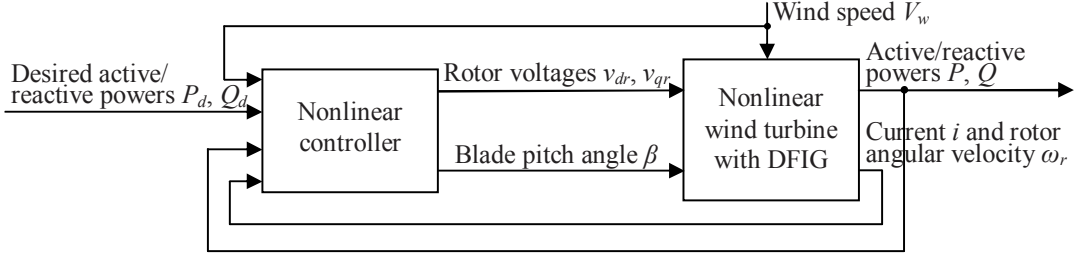


Fig. 2. Structure of the multivariable, feedback/feedforward nonlinear controller, developed based on original, nonlinear dynamics of the wind turbine.

we will assume, in the sequel, that K is chosen so that the electrical dynamics (33) are asymptotically stable and so fast that they may be approximated by (34).

B. Tracking of Desired Angular Velocity

The second step of the controller development involves constructing a speed controller that ensures the angular velocity of the rotor, ω_r , tracks a desired, time-varying reference, ω_{rd} , whenever possible. The construction may be divided into four substeps as described below.

Substep 1. First, we show that the electromagnetic torque T_e defined in (24) may be expressed as a *quadratic function* of the new control variables u_1 and u_2 . From (24) and (30),

$$\begin{aligned} T_e &= \varphi_{qs} i_{ds} - \varphi_{ds} i_{qs} = \begin{bmatrix} x_2 & -x_1 \end{bmatrix} \begin{bmatrix} i_{ds} \\ i_{qs} \end{bmatrix} \\ &= x^T \begin{bmatrix} 0 & -\frac{1}{\sigma L_s} & 0 & \frac{L_m}{\sigma L_s L_r} \\ \frac{1}{\sigma L_s} & 0 & -\frac{L_m}{\sigma L_s L_r} & 0 \\ 0 & 0 & 0 & 0 \\ 0 & 0 & 0 & 0 \end{bmatrix} x. \end{aligned} \quad (35)$$

Equation (35) suggests that T_e is a quadratic function of x , while (34) suggests that x , in turn, is an affine function of u_1 and u_2 , since v_{ds} and v_{qs} in (34) are assumed to be constants. Hence, T_e must be a quadratic function of u_1 and u_2 . Indeed, an explicit expression can be obtained as follows: since $A - BK$ is asymptotically stable and thus nonsingular, it may be written as

$$(A - BK)^{-1} = \begin{bmatrix} d_{11} & d_{12} & d_{13} & d_{14} \\ d_{21} & d_{22} & d_{23} & d_{24} \\ d_{31} & d_{32} & d_{33} & d_{34} \\ d_{41} & d_{42} & d_{43} & d_{44} \end{bmatrix}, \quad (36)$$

where each d_{ij} depends on A , B , and K . From (34)–(36),

$$\begin{aligned} T_e &= \frac{L_m}{\sigma L_s L_r} [(d_{11} v_{ds} + d_{12} v_{qs} + d_{13} u_1 + d_{14} u_2) \\ &\quad (d_{41} v_{ds} + d_{42} v_{qs} + d_{43} u_1 + d_{44} u_2) \\ &\quad - (d_{21} v_{ds} + d_{22} v_{qs} + d_{23} u_1 + d_{24} u_2) \\ &\quad (d_{31} v_{ds} + d_{32} v_{qs} + d_{33} u_1 + d_{34} u_2)] \\ &= \begin{bmatrix} u_1 & u_2 \end{bmatrix} \begin{bmatrix} q_1 & q_2 \\ q_2 & q_3 \end{bmatrix} \begin{bmatrix} u_1 \\ u_2 \end{bmatrix} + \begin{bmatrix} b_1 & b_2 \end{bmatrix} \begin{bmatrix} u_1 \\ u_2 \end{bmatrix} + a, \end{aligned} \quad (37)$$

where q_1 , q_2 , q_3 , b_1 , b_2 , and a are constants defined as

$$q_1 = \frac{L_m}{\sigma L_s L_r} (d_{13} d_{43} - d_{23} d_{33}), \quad (38)$$

$$q_2 = \frac{1}{2} \frac{L_m}{\sigma L_s L_r} (d_{13} d_{44} + d_{14} d_{43} - d_{23} d_{34} - d_{24} d_{33}), \quad (39)$$

$$q_3 = \frac{L_m}{\sigma L_s L_r} (d_{14} d_{44} - d_{24} d_{34}), \quad (40)$$

$$\begin{aligned} b_1 &= \frac{L_m}{\sigma L_s L_r} ((d_{11} v_{ds} + d_{12} v_{qs}) d_{43} + d_{13} (d_{41} v_{ds} + d_{42} v_{qs}) \\ &\quad - (d_{21} v_{ds} + d_{22} v_{qs}) d_{33} - d_{23} (d_{31} v_{ds} + d_{32} v_{qs})), \end{aligned} \quad (41)$$

$$\begin{aligned} b_2 &= \frac{L_m}{\sigma L_s L_r} ((d_{11} v_{ds} + d_{12} v_{qs}) d_{44} + d_{14} (d_{41} v_{ds} + d_{42} v_{qs}) \\ &\quad - (d_{21} v_{ds} + d_{22} v_{qs}) d_{34} - d_{24} (d_{31} v_{ds} + d_{32} v_{qs})), \end{aligned} \quad (42)$$

$$\begin{aligned} a &= \frac{L_m}{\sigma L_s L_r} ((d_{11} v_{ds} + d_{12} v_{qs}) (d_{41} v_{ds} + d_{42} v_{qs}) \\ &\quad - (d_{21} v_{ds} + d_{22} v_{qs}) (d_{31} v_{ds} + d_{32} v_{qs})). \end{aligned} \quad (43)$$

Substep 2. Next, we show that the quadratic function (37) relating u_1 and u_2 to T_e has a desirable feature: its associated Hessian matrix $\begin{bmatrix} q_1 & q_2 \\ q_2 & q_3 \end{bmatrix}$ is always *positive definite*, regardless of the parameters of the electrical part of the DFIG, as well as the choice of the state feedback gain matrix K . The following lemma formally states and proves this assertion:

Lemma 1. *The Hessian matrix $\begin{bmatrix} q_1 & q_2 \\ q_2 & q_3 \end{bmatrix}$ in (37) is positive definite.*

Proof: From (29), (33), (36), (38), (39), and (40), the determinant of $A - BK$ and the leading principal minors q_1 and $q_1 q_3 - q_2^2$ of $\begin{bmatrix} q_1 & q_2 \\ q_2 & q_3 \end{bmatrix}$ can be written as

$$|A - BK| = \frac{\Delta}{(L_s L_r - L_m^2)^2}, \quad (44)$$

$$q_1 = \frac{R_s L_m^2 (\Delta_1^2 + \Delta_2^2)}{\Delta^2}, \quad (45)$$

$$q_1 q_3 - q_2^2 = \frac{R_s^2 L_m^4}{\Delta^2}, \quad (46)$$

where

$$\begin{aligned} \Delta &= (-R_s L_m k_{12} + (L_s L_r - L_m^2) k_{13} - R_s L_r k_{14} \\ &\quad + R_r L_s + R_s L_r) \Delta_1 \\ &\quad + (R_s L_m k_{11} + R_s L_r k_{13} + (L_s L_r - L_m^2) k_{14} \\ &\quad + R_s R_r - L_s L_r + L_m^2) \Delta_2, \end{aligned} \quad (47)$$

$$\begin{aligned} \Delta_1 &= R_s L_m k_{21} + R_s L_r k_{23} + (L_s L_r - L_m^2) k_{24} \\ &\quad + R_r L_s + R_s L_r, \end{aligned}$$

$$\begin{aligned} \Delta_2 = & R_s L_m k_{22} + (-L_s L_r + L_m^2) k_{23} + R_s L_r k_{24} \\ & + R_s R_r - L_s L_r + L_m^2, \end{aligned}$$

and k_{ij} is the ij entry of K . Since $A - BK$ is nonsingular, $L_s > L_m$, and $L_r > L_m$, it follows from (44) that $\Delta \neq 0$. Since $\Delta \neq 0$, it follows from (46) that $q_1 q_3 - q_2^2 > 0$ and from (47) that Δ_1 and Δ_2 cannot be zero simultaneously. The latter, along with (45), implies that $q_1 > 0$. Since $q_1 > 0$ and $q_1 q_3 - q_2^2 > 0$, $\begin{bmatrix} q_1 & q_2 \\ q_2 & q_3 \end{bmatrix}$ in (37) must be positive definite. ■

Substep 3. Next, we show that there is a *redundancy* in the control variables u_1 and u_2 , which may be exposed via a *coordinate change*. Observe from (23) that the first-order dynamics of ω_r are driven by T_e . Also observe from Substeps 1 and 2 that T_e is a convex quadratic function of u_1 and u_2 . Thus, we have *two* coupled control inputs (i.e., u_1 and u_2) affecting *one* state variable (i.e., ω_r), implying that there is a redundancy in the control inputs, which may be exploited elsewhere (to be discussed in Section III-C). To expose this redundancy, first notice that because the Hessian matrix $\begin{bmatrix} q_1 & q_2 \\ q_2 & q_3 \end{bmatrix}$ is positive definite, it can be diagonalized, i.e., there exist an orthogonal matrix M containing its eigenvectors and a diagonal matrix D containing its eigenvalues, such that

$$M^T \begin{bmatrix} q_1 & q_2 \\ q_2 & q_3 \end{bmatrix} M = D. \quad (48)$$

Indeed,

$$M = \begin{bmatrix} \frac{q_2}{\sqrt{q_2^2 + (\lambda_1 - q_1)^2}} & \frac{\lambda_2 - q_3}{\sqrt{(\lambda_2 - q_3)^2 + q_2^2}} \\ \frac{\lambda_1 - q_1}{\sqrt{q_2^2 + (\lambda_1 - q_1)^2}} & \frac{q_2}{\sqrt{(\lambda_2 - q_3)^2 + q_2^2}} \end{bmatrix}, \quad D = \begin{bmatrix} \lambda_1 & 0 \\ 0 & \lambda_2 \end{bmatrix},$$

where

$$\lambda_{1,2} = \frac{q_1 + q_3 \pm \sqrt{(q_1 + q_3)^2 - 4(q_1 q_3 - q_2^2)}}{2}.$$

Next, consider the following coordinate change, which transforms $u_1 \in \mathbb{R}$ and $u_2 \in \mathbb{R}$ in a Cartesian coordinate system into $r \geq 0$ and $\theta \in [0, 2\pi)$ in a polar coordinate system:

$$r = \sqrt{z^T z}, \quad \theta = \tan^{-1} \left(\frac{z_2}{z_1} \right), \quad (49)$$

where

$$z = \begin{bmatrix} z_1 \\ z_2 \end{bmatrix} = D^{1/2} M^T \begin{bmatrix} u_1 \\ u_2 \end{bmatrix} + \frac{1}{2} D^{-1/2} M^T \begin{bmatrix} b_1 \\ b_2 \end{bmatrix}. \quad (50)$$

In terms of the new coordinates r and θ , it follows from (37) and (48)–(50) that

$$T_e = r^2 + a', \quad (51)$$

where

$$a' = a - \frac{1}{4} \begin{bmatrix} b_1 & b_2 \end{bmatrix} \begin{bmatrix} q_1 & q_2 \\ q_2 & q_3 \end{bmatrix}^{-1} \begin{bmatrix} b_1 \\ b_2 \end{bmatrix}.$$

Using (38)–(43), a' may be simplified to

$$a' = -\frac{v_{ds}^2 + v_{qs}^2}{4\omega_s R_s}, \quad (52)$$

implying that it is always negative. Comparing (51) with (37) shows that the coordinate change (49) and (50) allows us to decouple the control variables, so that in the new coordinates, r is responsible for driving the first-order dynamics of ω_r through

T_e of (51), while θ does not at all affect ω_r (and, hence, is redundant as far as the dynamics of ω_r are concerned). The design of r and θ will be discussed in Substep 4 and Section III-C, respectively.

Substep 4. Finally, a *speed controller* is presented, which ensures that the rotor angular velocity ω_r tracks a desired time-varying reference ω_{rd} , to be determined in Section III-C, provided that ω_{rd} is not exceedingly large. Combining (23) and (51) yields

$$J\dot{\omega}_r = T_m(\omega_r, \beta, V_w) - r^2 - a' - C_f \omega_r, \quad (53)$$

where, according to (25),

$$T_m(\omega_r, \beta, V_w) = \frac{\frac{1}{2} \rho A C_p(\lambda, \beta) V_w^3}{\omega_r}. \quad (54)$$

Here, T_m is written as $T_m(\omega_r, \beta, V_w)$ to emphasize its dependence on ω_r , β , and V_w . Observe from (53) that, if the control input r^2 were *real-valued* instead of being nonnegative, feedback linearization may be applied to cancel all the terms on the right-hand side of (53) and insert linear dynamics $\alpha(\omega_r - \omega_{rd})$, i.e., we may let

$$r^2 = T_m(\omega_r, \beta, V_w) - a' - C_f \omega_r + \alpha(\omega_r - \omega_{rd}), \quad (55)$$

so that

$$J\dot{\omega}_r = -\alpha(\omega_r - \omega_{rd}). \quad (56)$$

By letting the controller parameter α be positive, (56) implies that ω_r always attempts to go to ω_{rd} . Unfortunately, because r^2 cannot be negative, the speed controller (55)—and, hence, the linear dynamics (56)—cannot be realized whenever the right-hand side of (55) is negative. To alleviate this issue, (55) is slightly modified by setting r^2 to zero whenever that occurs, i.e.,

$$r^2 = \max\{T_m(\omega_r, \beta, V_w) - a' - C_f \omega_r + \alpha(\omega_r - \omega_{rd}), 0\}. \quad (57)$$

Notice that (57) contains a feedforward action involving the “disturbance”, i.e., the wind speed V_w . This explains the first input of the *nonlinear controller* block in Figure 2.

To analyze the behavior of the speed controller (57), suppose ω_{rd} , β , and V_w are constants and consider the function g , defined as

$$g(\omega_r, \beta, V_w) = T_m(\omega_r, \beta, V_w) - a' - C_f \omega_r. \quad (58)$$

The following lemma says that $g(\omega_r, \beta, V_w)$, when viewed as a function of ω_r , has a positive root $\omega_r^{(1)}$, below which $g(\omega_r, \beta, V_w)$ is positive:

Lemma 2. *For each fixed $\beta \in [\beta_{\min}, \beta_{\max}]$ and $V_w > 0$, there exists $\omega_r^{(1)} \in (0, \infty)$ such that $g(\omega_r^{(1)}, \beta, V_w) = 0$ and $g(\omega_r, \beta, V_w) > 0$ for all $\omega_r \in (0, \omega_r^{(1)})$.*

Proof: Due to the fact that a' in (52) is negative, there exists $\omega_{r,1}$ such that $-a' - C_f \omega_r > 0$ for all $\omega_r \in (0, \omega_{r,1})$. Due to Assumption (A3) of Section II, (26), and (54), there exists $\omega_{r,2}$ such that $T_m(\omega_r, \beta, V_w) > 0$ for all $\omega_r \in (0, \omega_{r,2})$. Hence, from (58), we have $g(\omega_r, \beta, V_w) > 0$ for all $\omega_r \in (0, \min\{\omega_{r,1}, \omega_{r,2}\})$. In addition, due to Assumption (A2),

(26), (54), (58), and $a' < 0$, there exists $\omega_{r,3}$, sufficiently large, such that $g(\omega_{r,3}, \beta, V_w) < 0$. These two properties of g , along with Assumption (A1) and the Intermediate Value Theorem, imply that there exists at least one positive root ω_r satisfying $g(\omega_r, \beta, V_w) = 0$. Letting $\omega_r^{(1)}$ be the first of such roots completes the proof. ■

The following theorem, derived based on Lemma 2, says that as long as the desired rotor angular velocity ω_{rd} is not exceedingly large, i.e., does not exceed the first root $\omega_r^{(1)}$ of $g(\omega_r, \beta, V_w)$, the closed-loop dynamics (53) and (57) have an asymptotically stable equilibrium point at ω_{rd} :

Theorem 1. Consider the first-order dynamics (53) and the speed controller (57). Suppose ω_{rd} , β , and V_w are constants, with ω_{rd} satisfying $0 < \omega_{rd} < \omega_r^{(1)}$. Then, for all $\omega_r(0) > 0$, $\lim_{t \rightarrow \infty} \omega_r(t) = \omega_{rd}$.

Proof: Substituting (57) into (53) and using (58) yield

$$J\dot{\omega}_r = \min\{\alpha(\omega_{rd} - \omega_r), g(\omega_r, \beta, V_w)\}. \quad (59)$$

Suppose $0 < \omega_{rd} < \omega_r^{(1)}$. We first show that $\omega_r = \omega_{rd}$ is the unique equilibrium point of (59). Suppose $\omega_r = \omega_{rd}$. Then, $\alpha(\omega_{rd} - \omega_r)$ in (59) is zero, whereas $g(\omega_r, \beta, V_w)$ in (59) is positive, due to Lemma 2. Thus, $\dot{\omega}_r = 0$, implying that ω_{rd} is an equilibrium point. Next, suppose $0 < \omega_r < \omega_{rd}$. Then, $\alpha(\omega_{rd} - \omega_r)$ is positive, and so is $g(\omega_r, \beta, V_w)$, due again to Lemma 2. Hence, $\dot{\omega}_r > 0$, implying that there is no equilibrium point to the left of ω_{rd} . Finally, suppose $\omega_r > \omega_{rd}$. Then, $\alpha(\omega_{rd} - \omega_r)$ is negative. Therefore, $\dot{\omega}_r < 0$, implying that there is no equilibrium point to the right of ω_{rd} . From the above analysis, we see that $\omega_r = \omega_{rd}$ is the unique equilibrium point of (59). Next, we show that the equilibrium point $\omega_r = \omega_{rd}$ is asymptotically stable in that for all $\omega_r(0) > 0$, $\lim_{t \rightarrow \infty} \omega_r(t) = \omega_{rd}$. Consider a quadratic Lyapunov function candidate $V : (0, \infty) \rightarrow \mathbb{R}$, defined as

$$V(\omega_r) = \frac{1}{2}(\omega_r - \omega_{rd})^2, \quad (60)$$

which is positive definite with respect to the shifted origin $\omega_r = \omega_{rd}$. From (59) and (60),

$$\dot{V}(\omega_r) = \frac{1}{J}(\omega_r - \omega_{rd}) \min\{\alpha(\omega_{rd} - \omega_r), g(\omega_r, \beta, V_w)\}. \quad (61)$$

Note that whenever $0 < \omega_r < \omega_{rd}$, $\alpha(\omega_{rd} - \omega_r) > 0$ and $g(\omega_r, \beta, V_w) > 0$, so that $\dot{V}(\omega_r) < 0$ according to (61). On the other hand, whenever $\omega_r > \omega_{rd}$, $\alpha(\omega_{rd} - \omega_r) < 0$, so that $\dot{V}(\omega_r) < 0$. Finally, when $\omega_r = \omega_{rd}$, $\dot{V}(\omega_r) = 0$. Therefore, $\dot{V}(\omega_r)$ is negative definite with respect to the shifted origin $\omega_r = \omega_{rd}$. It follows from [43] that $\omega_r = \omega_{rd}$ is asymptotically stable, i.e., for all $\omega_r(0) > 0$, $\lim_{t \rightarrow \infty} \omega_r(t) = \omega_{rd}$. ■

Theorem 1 says that the first root $\omega_r^{(1)}$ is a *critical root*, for which ω_{rd} should never exceed, if we want $\omega_r(t)$ to go to ω_{rd} regardless of $\omega_r(0)$. Figure 3 shows, for the MATLAB/Simulink R2007a model of $C_p(\lambda, \beta)$ given in (27) and (28), how the critical root $\omega_r^{(1)}$ depends on β and V_w . Notice from the figure that $\omega_r^{(1)}$ is insensitive to β but proportional to V_w , meaning that the larger the wind speed, the higher the ‘‘ceiling’’ on the desired rotor angular velocity. Also notice that

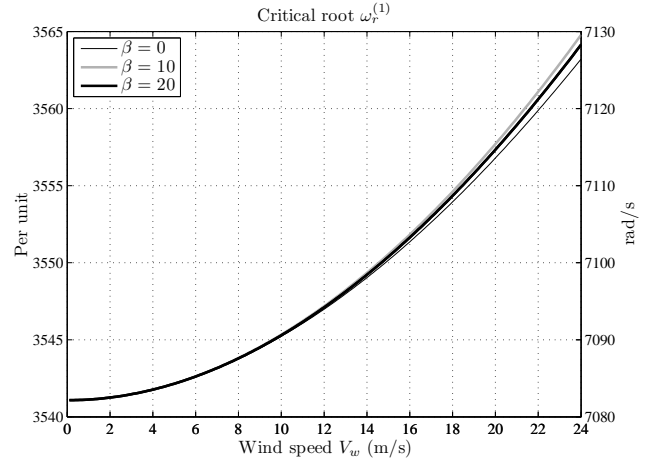


Fig. 3. Critical root $\omega_r^{(1)}$ as a function of blade pitch angle β and wind speed V_w .

$\omega_r^{(1)}$ of more than 3500 in the per-unit system is extremely large, meaning that for this particular turbine there is no need to be concerned about ω_{rd} exceeding $\omega_r^{(1)}$.

C. Lyapunov-like Function and Gradient-based Approach

The third and final step of the controller development involves introducing a Lyapunov-like function, which measures the difference between the actual and desired powers, and utilizing a gradient-based approach, which minimizes this function.

Recall from the beginning of Section III that the objective of the controller is to make the active and reactive powers, P and Q , track some desired references, P_d and Q_d , as closely as possible. In the MPT mode, where the goal is to generate as much active power as possible while maintaining an acceptable power factor, P_d is set to a value that far exceeds what the wind turbine can possibly produce (e.g., in the per-unit system, $P_d > 1$), while Q_d is set to a value representing the desired power factor $\text{PF}_d = \frac{P_d}{\sqrt{P_d^2 + Q_d^2}}$. In this mode, making P and Q approach P_d and Q_d is equivalent to maximizing the active power output while preserving the power factor. In the PR mode, where the goal is to regulate the powers, both P_d and Q_d are set to values representing power demands from the grid. In this mode, making P and Q approach P_d and Q_d amounts to achieving power regulation. Hence, the values of P_d and Q_d reflect the mode the wind farm operator wants the wind turbine to operate in. However, as far as the controller is concerned, it does not distinguish between the two modes; all it does is try its best to drive P and Q to P_d and Q_d .

To mathematically describe the aforementioned controller objective, consider the following positive definite, quadratic Lyapunov-like function V of the differences $P - P_d$ and $Q - Q_d$:

$$V = \frac{1}{2} \begin{bmatrix} P - P_d & Q - Q_d \end{bmatrix} \underbrace{\begin{bmatrix} w_p & w_{pq} \\ w_{pq} & w_q \end{bmatrix}}_{>0} \begin{bmatrix} P - P_d \\ Q - Q_d \end{bmatrix}, \quad (62)$$

where w_p , w_q , and w_{pq} are design parameters that allow one to specify how the differences $P - P_d$ and $Q - Q_d$, as well as

their correlation $(P - P_d)(Q - Q_d)$, should be penalized. With this V , the above controller objective can be restated simply as: *make V go to zero*, because when this happens, P and Q must both go to P_d and Q_d . Since it is not always possible to achieve this objective—due to the fact that the wind may not always be strong enough—below we will attempt instead to *make V as small as possible by minimizing it*.

To minimize V , we first show that V is a function of ω_{rd} , θ , β , V_w , P_d , and Q_d , i.e.,

$$V = f(\omega_{rd}, \theta, \beta, V_w, P_d, Q_d) \quad (63)$$

for some f . Note from (62) that V depends on P , Q , P_d , and Q_d . Also note from (17)–(20), (21), and (22) that P and Q , in turn, depend on i , v_{dr} , and v_{qr} (recall that v_{ds} and v_{qs} are constants). Thus,

$$V = f_1(i, v_{dr}, v_{qr}, P_d, Q_d) \quad (64)$$

for some f_1 . Next, note from (9)–(12) that i depends on x ; from (31) and (32) that v_{dr} and v_{qr} depend on x , ω_r , u_1 , and u_2 ; and from (34) that x further depends on u_1 and u_2 . Hence,

$$(i, v_{dr}, v_{qr}) = f_2(\omega_r, u_1, u_2) \quad (65)$$

for some f_2 . Furthermore, note from (49) and (50) that u_1 and u_2 depend on r and θ , where r , in turn, depends on ω_r , ω_{rd} , β , and V_w through (57). Therefore,

$$(u_1, u_2) = f_3(\omega_r, \omega_{rd}, \theta, \beta, V_w) \quad (66)$$

for some f_3 . Finally, assuming that ω_{rd} does not exceed the first root $\omega_r^{(1)}$ and assuming that ω_{rd} , β , and V_w are all relatively slow-varying (see below for a discussion), Theorem 1 says that ω_r goes to ω_{rd} . Thus, after a short transient,

$$\omega_r \approx \omega_{rd}. \quad (67)$$

Combining (64)–(67), (63) is obtained as claimed.

Now observe that the first three variables $(\omega_{rd}, \theta, \beta)$ in (63) are yet to be determined, while the last three variables (V_w, P_d, Q_d) are exogenous but known. Therefore, for each given (V_w, P_d, Q_d) , $(\omega_{rd}, \theta, \beta)$ can be chosen correspondingly in order to minimize V . This defines a mapping from (V_w, P_d, Q_d) to $(\omega_{rd}, \theta, \beta)$, i.e.,

$$\begin{aligned} (\omega_{rd}, \theta, \beta) &= F(V_w, P_d, Q_d) \\ &\triangleq \arg \min_{(x_1, x_2, x_3)} f(x_1, x_2, x_3, V_w, P_d, Q_d). \end{aligned} \quad (68)$$

In principle, the mapping F in (68) may be constructed either *analytically*, by setting the gradient of $f(\cdot)$ to zero and solving for the minimizer $(\omega_{rd}, \theta, \beta)$ in terms of (V_w, P_d, Q_d) , or *numerically*, by means of a three-dimensional lookup table. Unfortunately, the former is difficult to carry out, since f , being composed of several nonlinear transformations (64)–(67), has a rather complex expression. On the other hand, the latter is costly to generate and can easily become obsolete due to variations in system parameters. More important, selecting $(\omega_{rd}, \theta, \beta)$ as a *static* function of (V_w, P_d, Q_d) as in (68) may lead to steep jumps in $(\omega_{rd}, \theta, \beta)$ because V_w is ever-changing and may change dramatically, and both P_d and Q_d from the wind farm operator may experience step changes. Such steep jumps are undesirable because large fluctuations

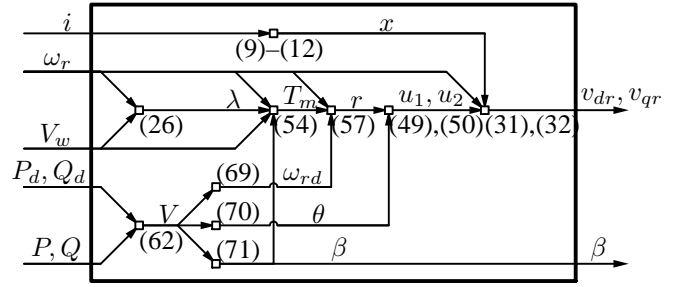


Fig. 4. Internal structure of the proposed nonlinear controller.

in ω_{rd} may prevent ω_r from tracking it, while discontinuous changes in β may be mechanically impossible to realize, cause intolerable vibrations, and substantially cut short the lifetime of the turbine blades.

To alleviate the aforementioned deficiencies of selecting $(\omega_{rd}, \theta, \beta)$ according to (68), a gradient-based approach is considered for updating $(\omega_{rd}, \theta, \beta)$:

$$\dot{\omega}_{rd} = -\epsilon_1 \frac{\partial f}{\partial \omega_{rd}}, \quad (69)$$

$$\dot{\theta} = -\epsilon_2 \frac{\partial f}{\partial \theta}, \quad (70)$$

$$\dot{\beta} = -\epsilon_3 \frac{\partial f}{\partial \beta}, \quad (71)$$

where $\epsilon_1, \epsilon_2, \epsilon_3 > 0$ are design parameters, which are meant to be relatively small, especially ϵ_1 and ϵ_3 , in order to avoid steep changes in ω_{rd} and β . The partial derivatives $\frac{\partial f}{\partial \omega_{rd}}$, $\frac{\partial f}{\partial \theta}$, and $\frac{\partial f}{\partial \beta}$ in (69)–(71) can be calculated in a straightforward manner using (64)–(67), but are omitted from this paper due to space limitations. These partial derivatives are practically implementable since, like f , they depend on ω_{rd} , θ , β , V_w , P_d , and Q_d , all of which are known. With this gradient-based approach, $(\omega_{rd}, \theta, \beta)$ is guaranteed to asymptotically converge to a local minimum when (V_w, P_d, Q_d) is constant, and track a local minimum when (V_w, P_d, Q_d) varies.

To help the readers better understand the proposed nonlinear controller depicted in Figure 2 and described in this section, the internal structure of this controller is revealed in Figure 4. Observe that each arrow in this figure represents a signal, whereas each tiny box represents equations relating the signals.

IV. SIMULATION STUDIES

To demonstrate the effectiveness of the controller presented above, MATLAB simulations have been carried out, in which the controller is applied to a 1.5 MW GE turbine with 575 V base voltage and 60 Hz base frequency. To describe settings and results of the simulations, both the per-unit system and the physical unit system will be used, given that they are popular in the literature.

The simulation settings are as follows: All values of the wind turbine parameters are taken from the Wind Turbine Block of the Distributed Resources Library in MATLAB/Simulink R2007a. Specifically, the values are: $\omega_s(\text{pu}) = 1$, $R_s(\text{pu}) = 0.00706$, $R_r(\text{pu}) = 0.005$, $L_s(\text{pu}) = 3.071$, $L_r(\text{pu}) = 3.056$, $L_m(\text{pu}) = 2.9$, $J(\text{pu}) = 10.08$, $C_f(\text{pu}) = 0.01$, $\lambda_{\text{nom}} = 8.1$, and $C_{p_{\text{nom}}} = 0.48$. In addition, the

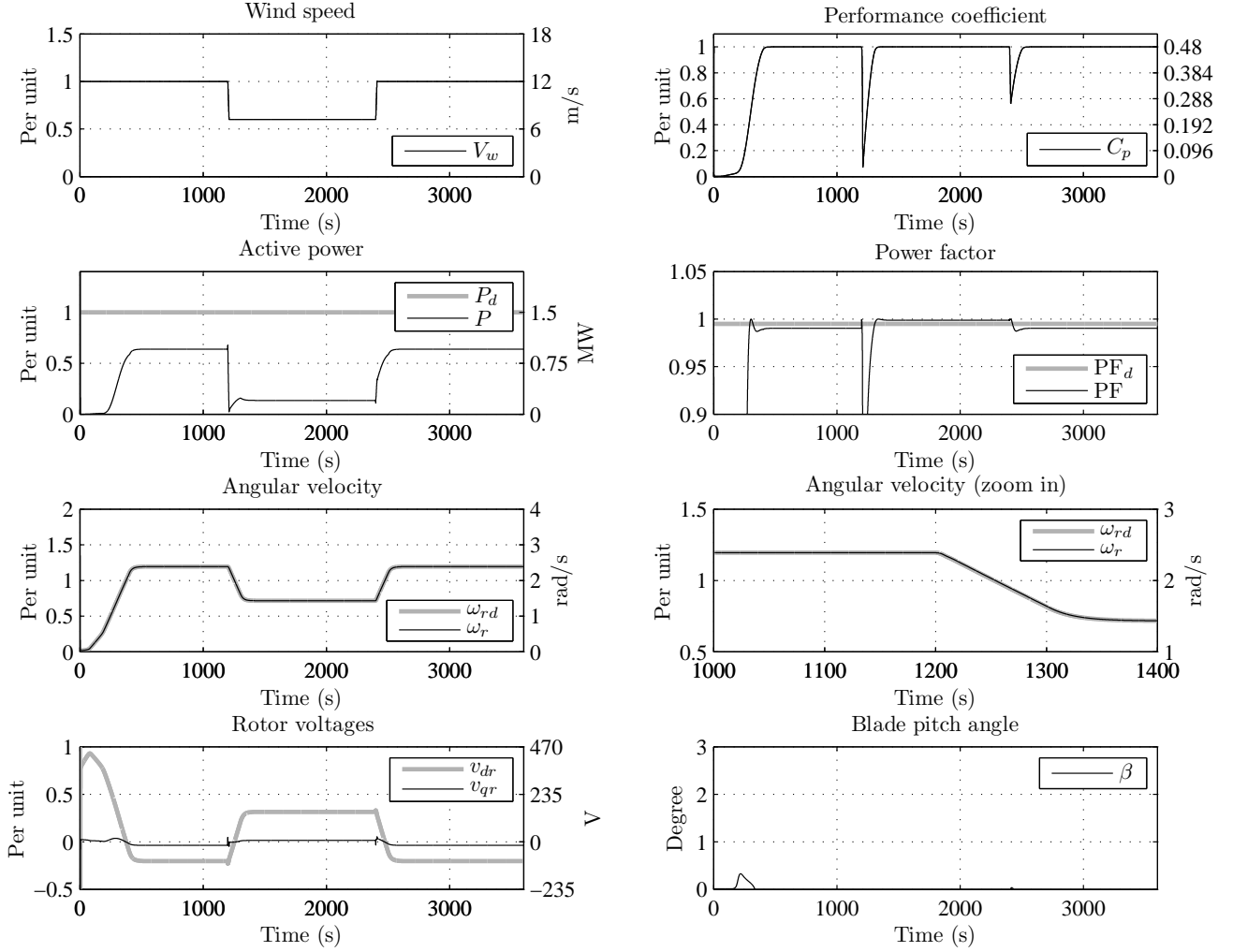


Fig. 5. Scenario 1 illustrating the maximum power tracking (MPT) mode.

base wind speed is $V_{w_base} = 12$ m/s. In MATLAB/Simulink R2007a, the mechanical power captured is given by

$$P_m(\text{pu}) = \frac{P_{\text{wind_base}} P_{\text{nom}}}{P_{\text{elec_base}}} C_p(\text{pu}) V_w(\text{pu})^3, \quad (72)$$

where $P_{\text{wind_base}} = 1.5$ MW, $P_{\text{nom}} = 0.73$, and $P_{\text{elec_base}} = 1.5 \times 10^6 / 0.9$ VA. From (72), it can be seen that at the base wind speed $V_w(\text{pu}) = 1$, $P_m(\text{pu})$ is capped at 0.657. Furthermore, without loss of generality, the constant stator voltages are set to $v_{ds}(\text{pu}) = 1$ and $v_{qs}(\text{pu}) = 0$.

For the proposed controller, we let the desired poles of the electrical dynamics (33) be located at -15 , -5 , and $-10 \pm 5j$, so that the corresponding state feedback gain matrix K , calculated using MATLAB's `place()` function, is

$$K = \begin{bmatrix} 5135.9 & 259.2 & 20.3 & 1.9 \\ -2676.7 & 4289.9 & -1.3 & 19.7 \end{bmatrix}.$$

In addition, we let $w_p = 10$, $w_q = 1$, and $w_{pq} = 0$, implying that we penalize the difference between P and P_d much more than we do Q and Q_d . Finally, we choose the rest of the controller parameters as follows: $\alpha = 10$, $\epsilon_1 = 4 \times 10^{-3}$, $\epsilon_2 = 1 \times 10^{-4}$, and $\epsilon_3 = 2$.

Based on the above wind turbine and controller parameters, simulations have been carried out for four different scenarios. Description of each scenario, along with the simulation result, is given below:

Scenario 1: Maximum power tracking (MPT) mode. In this scenario, we simulate the situation where the wind speed V_w experiences step changes between 12 m/s and 7.2 m/s, while the desired powers P_d and Q_d are kept constant at 1.5 MW and 0.15 MW, so that the desired power factor is $\text{PF}_d = 0.995$. Since P_m cannot exceed 0.657×1.5 MW at the base wind speed $V_{w_base} = 12$ m/s, the wind turbine is expected to operate in the MPT mode. Figure 5 shows the simulation result for this scenario, where the key signals are plotted as functions of time in both the per-unit and physical unit systems wherever applicable. Observe that, after a short transient, the wind turbine converts as much wind energy to electric energy as it possibly could, as indicated by C_p approaching its maximum value of 0.48 in subplot 2 (which translates into P approaching its maximum possible value in subplot 3). Also observe that, when V_w goes from 12 m/s to 7.2 m/s and from 7.2 m/s back to 12 m/s, C_p drops sharply but quickly returns to its maximum value. Note from subplot

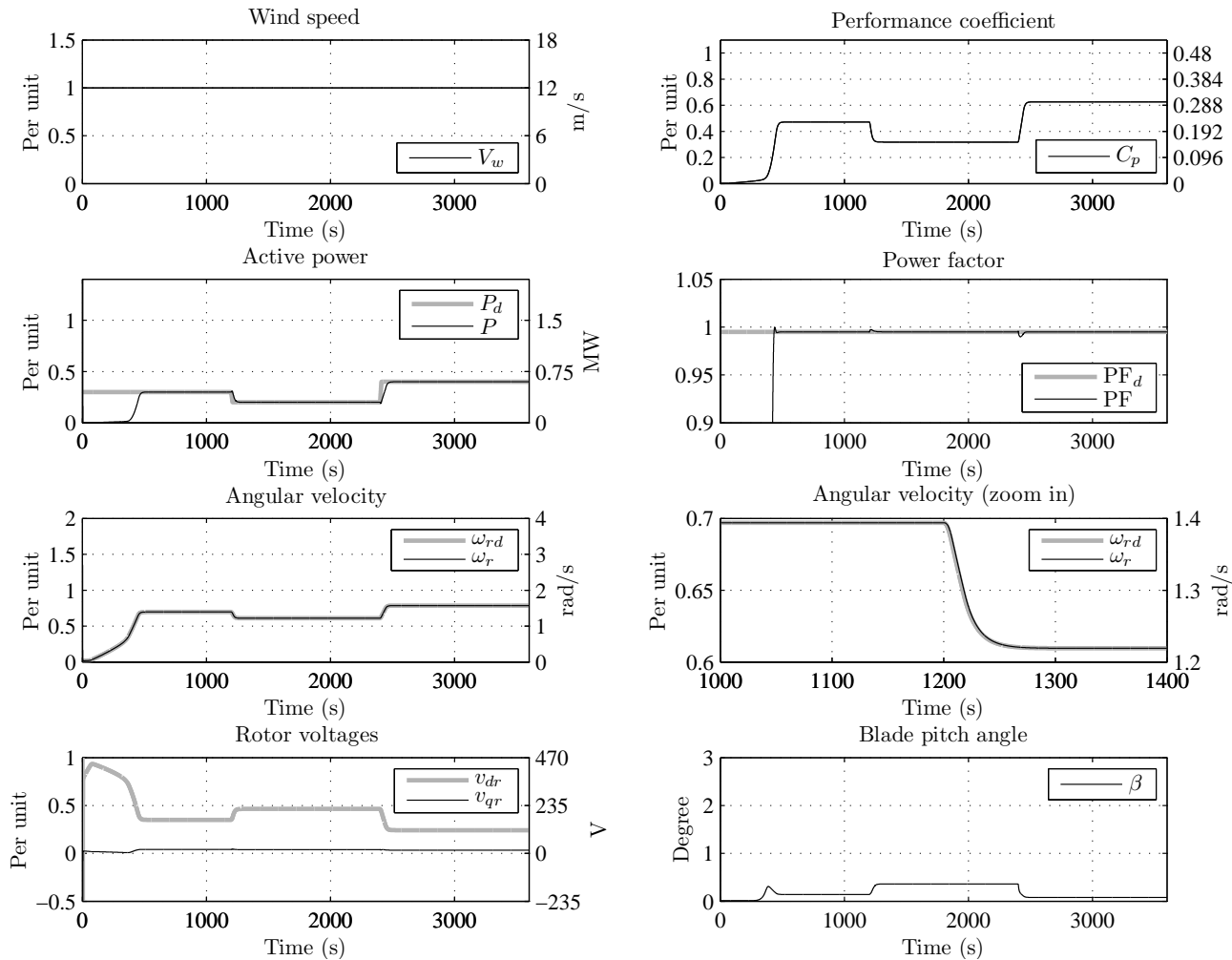


Fig. 6. Scenario 2 illustrating the power regulation (PR) mode.

4 that, regardless of V_w , the power factor PF is maintained near the desired level of 0.995. Moreover, note from subplots 5 and 6 that the angular velocity ω_r tracks the desired time-varying reference ω_{rd} closely (subplot 6 is a zoom-in version of subplot 5). Finally, the control inputs v_{dr} , v_{qr} , and β are shown in subplots 7 and 8, respectively. Note that, to maximize C_p , β is kept at its minimum value $\beta_{\min} = 0$ deg.

Scenario 2: Power regulation (PR) mode. In this scenario, we simulate the situation where V_w is kept constant at the base value of 12 m/s, while P_d experiences step changes from 0.45 MW to 0.3 MW and then to 0.6 MW, and Q_d is such that $PF_d = 0.995$. Since P_d is always less than 0.657×1.5 MW at the base wind speed of 12 m/s, the wind turbine is expected to operate in the PR mode with different setpoints P_d . Figure 6 shows the simulation result for this scenario. Observe from subplot 2 that C_p is less than its maximum value of 0.48. This suggests that the wind turbine attempts to capture less power than what it possibly could from wind, since P_d is relatively small. Indeed, as can be seen from subplots 3 and 4, the turbine produces just enough active and reactive powers, making P track P_d closely while maintaining PF at PF_d . Also observe from subplots 5 and 6 that ω_r closely follows ω_{rd} , as desired. Finally, note from subplot 8 that β increases slightly

in order to capture less power between 1200s and 2400s, when P_d is smallest.

Scenario 3: Seamless switching between the MPT and PR modes. In this scenario, we simulate the situation where P_d experiences large step changes between 1.5 MW and 0.75 MW, Q_d again is such that PF_d is 0.995, and an actual wind profile from a wind farm located in northwest Oklahoma is used to define V_w . The actual wind profile consists of 145 samples, taken at the rate of one sample per 10 minutes, over a 24-hour period. In order to use this wind profile in a 1-hour simulation (as in Scenarios 1 and 2), we compress the time scale, assuming that the samples were taken over a 1-hour period. Note that compressing the time scale in this way makes the problem more challenging because the wind speed varies faster than it actually does. Figure 7 shows the simulation result for this scenario, with subplot 1 displaying the wind profile. Observe from subplots 2 and 3 that, for the first 1200 seconds during which P_d is 1.5 MW, the turbine operates in the MPT mode, grabbing as much wind energy as it possibly could, by driving C_p to 0.48 and maximizing P . At time 1200s when P_d abruptly drops from 1.5 MW to 0.75 MW, the turbine seamlessly switches from the MPT mode to the PR mode, quickly reducing C_p , accurately regulating P around

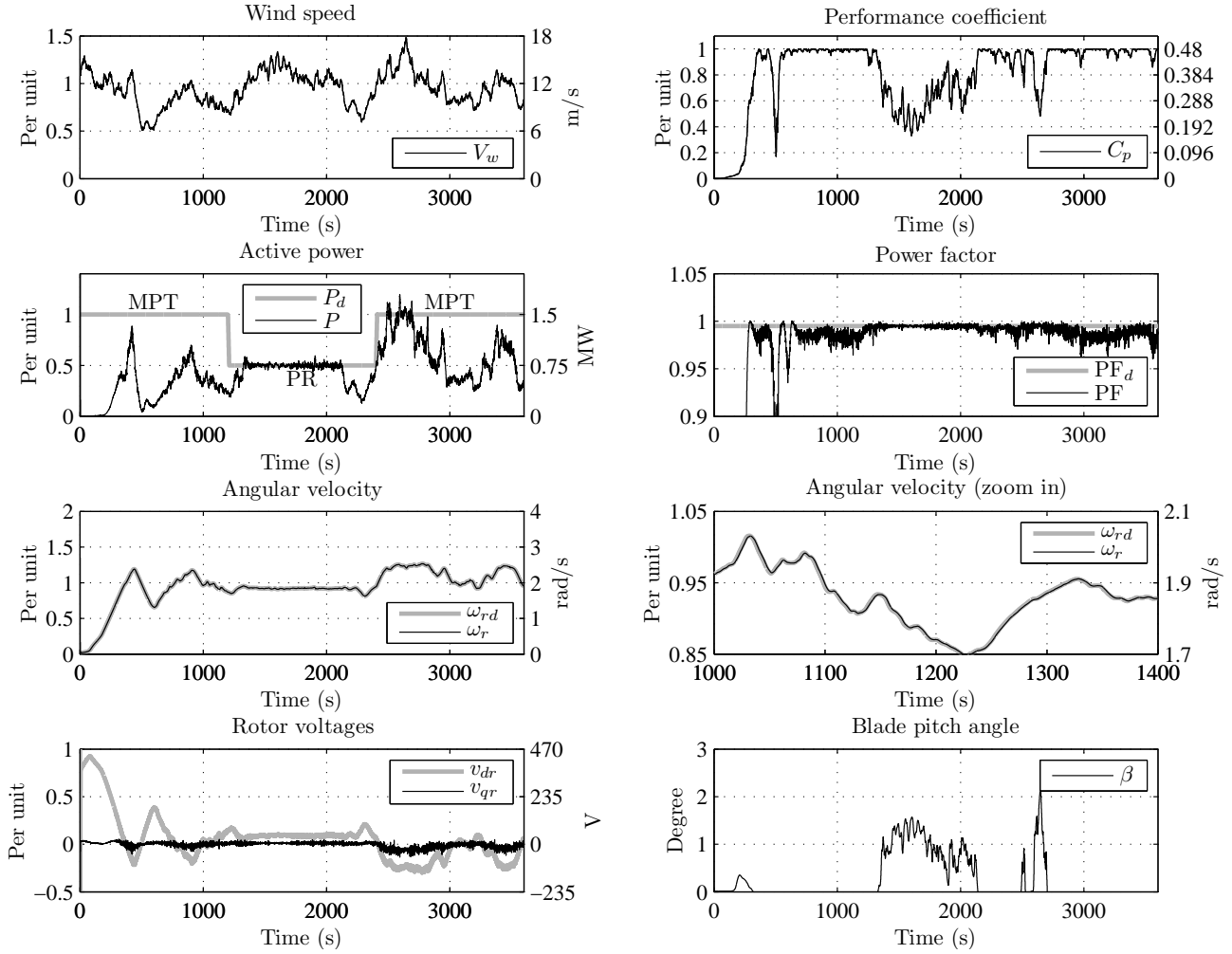


Fig. 7. Scenario 3 illustrating the seamless switching between the MPT and PR modes under an actual wind profile from a wind farm located in northwest Oklahoma.

P_d , and effectively rejecting the “disturbance” V_w . Note that between 2100s and 2400s, the wind is not strong enough to sustain the PR mode. As a result, the MPT mode resumes seamlessly, as indicated by C_p returning immediately to its maximum value of 0.48. Finally, at time 2400s when P_d goes from 0.75 MW back to 1.5 MW, the turbine keeps working in the MPT mode, continuing to maximize both C_p and P . Notice from subplots 4–6 that, over the course of the simulation, both PF and ω_r are maintained at PF_d and ω_{rd} , respectively, despite the random wind fluctuations. Also notice from subplot 8 that β increases somewhat during the PR mode in order to help capture less power.

Scenario 4: Robustness of the proposed controller. In this scenario, we simulate the exact same situation as that of Scenario 3 (i.e., with the same V_w , P_d , and Q_d) but with modeling errors and measurement noise. That is, we allow for modeling errors in the friction coefficient C_f and the performance coefficient C_p (due, for example, to changing weather conditions, blade erosions, and aging) as well as measurement noise in the wind speed V_w (since V_w is usually measured by an anemometer located on the nacelle behind the blades of a wind turbine). Specifically, we assume that

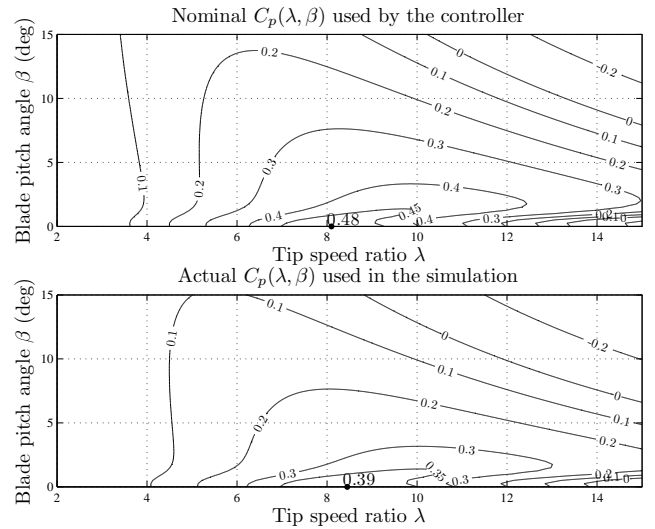


Fig. 8. Contour plots of the nominal and actual $C_p(\lambda, \beta)$ for Scenario 4.

the nominal C_f used by the controller is 0.01(pu), whereas the actual C_f used in the simulation is 0.012(pu), so that

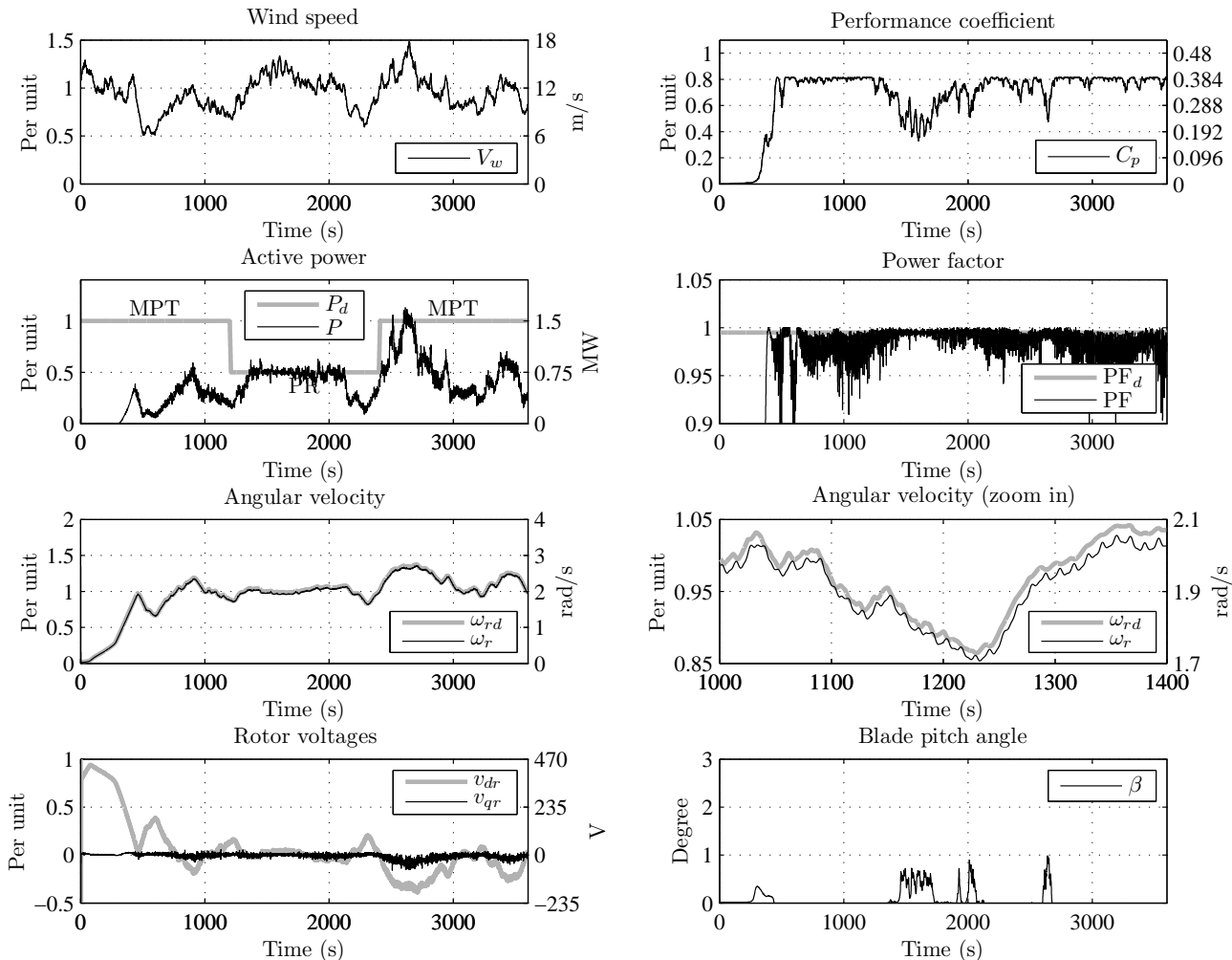


Fig. 9. Scenario 4 illustrating the robustness of the proposed controller to modeling errors in C_f and C_p and noisy measurements in V_w .

C_f has a 20% modeling error. Moreover, we assume that the nominal C_p used by the controller is given by (27) and (28) with $c_1 = 0.5176$, $c_2 = 116$, $c_3 = 0.4$, $c_4 = 5$, $c_5 = 21$, and $c_6 = 0.0068$, whereas the actual C_p used in the simulation is also given by (27) and (28) but with $c_1 = 0.45$, $c_2 = 115$, $c_3 = 0.5$, $c_4 = 4.5$, $c_5 = 22$, and $c_6 = 0.003$. Figure 8 displays the contour plots of the nominal and actual $C_p(\lambda, \beta)$ for $\lambda \in [2, 15]$ and $\beta \in [0, 15]$, showing that C_p has noticeable modeling errors. In particular, the nominal C_p attains its maximum of 0.48 at $(\lambda, \beta) = (8.1, 0)$, whereas the actual C_p attains its maximum of 0.39 at $(\lambda, \beta) = (8.45, 0)$. Finally, we assume that the measured V_w used by the controller, denoted as V_{w_meas} , is related to the actual V_w used in the simulation via

$$V_{w_meas}(t) = V_w(t) + 0.5 + 0.5 \sin(0.5t) + 0.25 \cos(t),$$

where the second term on the right-hand side represents a constant measurement bias, while the third and fourth represent measurement noises with different amplitudes and frequencies. Figure 9 shows the simulation result for this scenario. Comparing this figure with Figure 7, the following observations can be made: first, C_p in Figure 9 attains its maximum value of 0.39 in the MPT mode, as opposed to the

0.48 attained by C_p in Figure 7. Second, PF in Figure 9 has a larger fluctuation compared to PF in Figure 7, but nonetheless is maintained around PF_d . Third, ω_r in Figure 9 does not track ω_{rd} as closely as ω_r in Figure 7 does. Nevertheless, despite the wind fluctuations, modeling errors, and noisy measurements, the controller performs reasonably well, as evident by how close C_p is to its maximum value of 0.39 in the MPT mode, how close P is to P_d in the PR mode, and how close PF is to PF_d throughout the simulation. Therefore, the controller is fairly robust.

As it follows from Figures 5–9 and the above discussions, the proposed controller exhibits excellent performance. Specifically, the controller works well in both the MPT mode under step changes in the wind speed (Scenario 1) and the PR mode under step changes in the power commands (Scenario 2). In addition, it is capable of seamlessly switching between the two modes in the presence of changing power commands and a realistic, fluctuating wind profile (Scenario 3). Finally, the controller is robust to small modeling errors and noisy measurements commonly encountered in practice (Scenario 4).

V. CONCLUSION

In this paper, we have developed a feedback/feedforward nonlinear controller, which accounts for the nonlinearities of variable-speed wind turbines with doubly fed induction generators, and bypasses the need for approximate linearization. Its development is based on applying a mixture of linear and nonlinear control design techniques on three time scales, including feedback linearization, pole placement, and gradient-based minimization of a Lyapunov-like potential function. Simulation results have shown that the proposed scheme not only effectively controls the active and reactive powers in both the MPT and PR modes, it also ensures seamless switching between the two modes. Therefore, the proposed controller may be recommended as a candidate for future wind turbine control.

REFERENCES

- [1] P. B. Eriksen, T. Ackermann, H. Abildgaard, P. Smith, W. Winter, and J. M. Rodríguez García, "System operation with high wind penetration," *IEEE Power and Energy Magazine*, vol. 3, no. 6, pp. 65–74, 2005.
- [2] "20% wind energy by 2030—increasing wind energy's contribution to U.S. electricity supply," U.S. Department of Energy, Washington, DC, Executive Summary, 2008.
- [3] "Interim report—system disturbance on 4 November 2006," Union for the Co-Ordination of Transmission of Electricity, Brussels, Belgium, Executive Summary, 2006.
- [4] M. A. M. Prats, J. M. Carrasco, E. Galvan, J. A. Sanchez, L. G. Franquelo, and C. Batista, "Improving transition between power optimization and power limitation of variable speed, variable pitch wind turbines using fuzzy control techniques," in *Proc. Conference of the Industrial Electronics Society*, Nagoya, Japan, 2000, pp. 1497–1502.
- [5] E. Iyasere, M. Salah, D. Dawson, and J. Wagner, "Nonlinear robust control to maximize energy capture in a variable speed wind turbine," in *Proc. American Control Conference*, Seattle, WA, 2008, pp. 1824–1829.
- [6] K. E. Johnson, L. J. Fingersh, M. J. Balas, and L. Y. Pao, "Methods for increasing region 2 power capture on a variable-speed wind turbine," *Journal of Solar Energy Engineering*, vol. 126, no. 4, pp. 1092–1100, 2004.
- [7] K. E. Johnson, L. Y. Pao, M. J. Balas, and L. J. Fingersh, "Control of variable-speed wind turbines: standard and adaptive techniques for maximizing energy capture," *IEEE Control Systems Magazine*, vol. 26, no. 3, pp. 70–81, 2006.
- [8] V. Calderaro, V. Galdi, A. Piccolo, and P. Siano, "Design and implementation of a fuzzy controller for wind generators performance optimisation," in *Proc. European Conference on Power Electronics and Applications*, Aalborg, Denmark, 2007, pp. 1–10.
- [9] V. Galdi, A. Piccolo, and P. Siano, "Designing an adaptive fuzzy controller for maximum wind energy extraction," *IEEE Transactions on Energy Conversion*, vol. 23, no. 2, pp. 559–569, 2008.
- [10] R. B. Chedid, S. H. Karaki, and C. El-Chamali, "Adaptive fuzzy control for wind-diesel weak power systems," *IEEE Transactions on Energy Conversion*, vol. 15, no. 1, pp. 71–78, 2000.
- [11] B. Beltran, T. Ahmed-Ali, and M. E. H. Benbouzid, "Sliding mode power control of variable-speed wind energy conversion systems," *IEEE Transactions on Energy Conversion*, vol. 23, no. 2, pp. 551–558, 2008.
- [12] B. Malinga, J. Sneckenberger, and J. Feliachi, "Modeling and control of a wind turbine as a distributed resource," in *Proc. Southeastern Symposium on System Theory*, Morgantown, WV, 2003, pp. 108–112.
- [13] M. M. Hand and M. J. Balas, "Non-linear and linear model based controller design for variable-speed wind turbines," in *Proc. ASME/JSME Joint Fluids Engineering Conference*, San Francisco, CA, 1999, pp. 18–23.
- [14] L. Zhang, H. Li, C. E. J. Li, and H. Xu, "Pitch control of large scale wind turbine based on fuzzy-PD method," in *Proc. International Conference on Electric Utility Deregulation and Restructuring and Power Technologies*, Nanjing, China, 2008, pp. 2447–2452.
- [15] H. Geng and G. Yang, "Robust pitch controller for output power levelling of variable-speed variable-pitch wind turbine generator systems," *IET Renewable Power Generation*, vol. 3, no. 2, pp. 168–179, 2009.
- [16] E. Muljadi and C. P. Butterfield, "Pitch-controlled variable-speed wind turbine generation," *IEEE Transactions on Industry Applications*, vol. 37, no. 1, pp. 240–246, 2001.
- [17] T. Senjyu, R. Sakamoto, N. Urasaki, T. Funabashi, H. Fujita, and H. Sekine, "Output power leveling of wind turbine generator for all operating regions by pitch angle control," *IEEE Transactions on Energy Conversion*, vol. 21, no. 2, pp. 467–475, 2006.
- [18] K. Stol and M. J. Balas, "Full-state feedback control of a variable-speed wind turbine: A comparison of periodic and constant gains," *Journal of Solar Energy Engineering*, vol. 123, no. 4, pp. 319–326, 2001.
- [19] A. D. Wright and M. J. Balas, "Design of state-space-based control algorithms for wind turbine speed regulation," *Journal of Solar Energy Engineering*, vol. 125, no. 4, pp. 386–395, 2003.
- [20] —, "Design of modern controls for the controlled advanced research turbine (CART)," in *Proc. ASME Wind Energy Symposium*, Reno, NV, 2003, pp. 304–316.
- [21] J. Zhang, M. Cheng, Z. Chen, and X. Fu, "Pitch angle control for variable speed wind turbines," in *Proc. International Conference on Electric Utility Deregulation and Restructuring and Power Technologies*, Nanjing, China, 2008, pp. 2691–2696.
- [22] N. A. Janssens, G. Lambin, and N. Bragard, "Active power control strategies of DFIG wind turbines," in *Proc. IEEE Power Tech*, Lausanne, Switzerland, 2007, pp. 516–521.
- [23] G. C. Tarnowski and R. Reginatto, "Adding active power regulation to wind farms with variable speed induction generators," in *Proc. IEEE Power Engineering Society General Meeting*, Tampa, FL, 2007, pp. 1–8.
- [24] H.-S. Ko, G.-G. Yoon, and W.-P. Hong, "Active use of DFIG-based variable-speed wind-turbine for voltage regulation at a remote location," *IEEE Transactions on Power Systems*, vol. 22, no. 4, pp. 1916–1925, 2007.
- [25] T. Brekken and N. Mohan, "A novel doubly-fed induction wind generator control scheme for reactive power control and torque pulsation compensation under unbalanced grid voltage conditions," in *Proc. IEEE Power Electronics Specialist Conference*, Acapulco, Mexico, 2003, pp. 760–764.
- [26] B. Marinescu, "A robust coordinated control of the doubly-fed induction machine for wind turbines: a state-space based approach," in *Proc. American Control Conference*, Boston, MA, 2004, pp. 174–179.
- [27] D. D. Li and C. Chen, "Decoupled control of speed and reactive power of doubly-fed induction generator," in *Proc. International Conference on Power System Technology*, Singapore, 2004, pp. 356–360.
- [28] D. Zhi and L. Xu, "Direct power control of DFIG with constant switching frequency and improved transient performance," *IEEE Transactions on Energy Conversion*, vol. 22, no. 1, pp. 110–118, 2007.
- [29] F. Wu, X. Zhang, P. Ju, and M. J. H. Sterling, "Decentralized nonlinear control of wind turbine with doubly fed induction generator," *IEEE Transactions on Power Systems*, vol. 23, no. 2, pp. 613–621, 2008.
- [30] I. M. de Alegria, J. Andreu, P. Ibanez, J. L. Villate, and I. Gabiola, "Novel power error vector control for wind turbine with doubly fed induction generator," in *Proc. Conference of the IEEE Industrial Electronics Society*, Busan, South Korea, 2004, pp. 1218–1223.
- [31] R. Pena, J. C. Clare, and G. M. Asher, "Doubly fed induction generator using back-to-back PWM converters and its application to variable-speed wind-energy generation," *IEE Proc. Electric Power Applications*, vol. 143, no. 3, pp. 231–241, 1996.
- [32] B. Hopfensperger, D. J. Atkinson, and R. A. Lakin, "Stator-flux-oriented control of a doubly-fed induction machine with and without position encoder," *IEE Proc. Electric Power Applications*, vol. 147, no. 4, pp. 241–250, 2000.
- [33] A. Monroy, L. Alvarez-Icaza, and G. Espinosa-Perez, "Passivity-based control for variable speed constant frequency operation of a DFIG wind turbine," *International Journal of Control*, vol. 81, no. 9, pp. 1399–1407, 2008.
- [34] S. Peresada, A. Tilli, and A. Tonielli, "Power control of a doubly fed induction machine via output feedback," *Control Engineering Practice*, vol. 12, pp. 41–57, 2004.
- [35] B. Rabelo and W. Hofmann, "Optimal active and reactive power control with the doubly-fed induction generator in the MW-class wind-turbines," in *Proc. IEEE International Conference on Power Electronics and Drive Systems*, Bali, Indonesia, 2001, pp. 53–58.
- [36] H. Li, Z. Chen, and J. K. Pedersen, "Optimal power control strategy of maximizing wind energy tracking and conversion for VSCF doubly fed induction generator system," in *Proc. CES/IEEE International Power Electronics and Motion Control Conference*, Shanghai, China, 2006, pp. 1–6.

- [37] A. D. Hansen, P. Sorensen, F. Iov, and F. Blaabjerg, "Control of variable speed wind turbines with doubly-fed induction generators," *Wind Engineering*, vol. 28, no. 4, pp. 411–434, 2004.
- [38] B. K. Bose, *Modern Power Electronics and AC Drives*. Upper Saddle River, NJ: Prentice Hall PTR, 2002.
- [39] R. Fadaeinedjad, M. Moallem, and G. Moschopoulos, "Simulation of a wind turbine with doubly-fed induction generator by FAST and Simulink," *IEEE Transactions on Energy Conversion*, vol. 23, no. 2, pp. 690–700, 2008.
- [40] Y. Lei, A. Mullane, G. Lightbody, and R. Yacamini, "Modeling of the wind turbine with a doubly fed induction generator for grid integration studies," *IEEE Transactions on Energy Conversion*, vol. 21, no. 1, pp. 257–264, 2006.
- [41] F. D. Bianchi, H. De Battista, and R. J. Mantz, *Wind Turbine Control Systems: Principles, Modelling, and Gain Scheduling Design*. London, England: Springer, 2007.
- [42] S. Heier, *Grid Integration of Wind Energy Conversion Systems*. New York, NY: John Wiley & Sons, 1998.
- [43] H. K. Khalil, *Nonlinear Systems*, 3rd ed. Upper Saddle River, NJ: Prentice Hall, 2001.
- [44] C.-T. Chen, *Linear System Theory and Design*, 3rd ed. New York, NY: Oxford University Press, 1999.

Choon Yik Tang (S'97–M'04) received the B.S. and M.S. degrees in mechanical engineering from Oklahoma State University, Stillwater, in 1996 and 1997, respectively, and the Ph.D. degree in electrical engineering from the University of Michigan, Ann Arbor, in 2003. From 2003 to 2004, he was a Postdoctoral Research Fellow in the Department of Electrical Engineering and Computer Science at the University of Michigan. From 2004 to 2006, he was a Research Scientist at Honeywell Labs, Minneapolis. Since 2006, he has been an Assistant Professor in the School of Electrical and Computer Engineering at the University of Oklahoma, Norman. His current research interests include systems and control theory, distributed algorithms for computation and optimization over networks, and control and operation of wind farms.

Yi Guo (S'08) received the B.S. degree from Tianjin Polytechnic University, Tianjin, China, and the M.S. degree from Tianjin University, Tianjin, China, in 2002 and 2005, respectively. He is currently working toward his Ph.D. degree in the School of Electrical and Computer Engineering at the University of Oklahoma, Norman. His current research interests include control theory and applications, with an emphasis on control of wind turbines and wind farms.

John N. Jiang (SM'07) is an Assistant Professor in the Power System Group in the School of Electrical and Computer Engineering at the University of Oklahoma, Norman. He holds M.S. and Ph.D. degrees from the University of Texas at Austin. He has been involved in a number of wind energy related projects since 1989 in design, installation of stand-alone wind generation systems, the market impact of wind generation in Texas, and recent large-scale wind farms development in Oklahoma.